ON SOLVING FRICTIONAL CONTACT PROBLEMS PART II: DYNAMIC CASE

HERIBERT BLUM[1], HEIKO KLEEMANN[1], ANDREAS RADEMACHER[1], AND ANDREAS SCHRÖDER[2]

Abstract. Solution techniques for dynamic contact problems, namely dynamic Signorini problems with and without friction, thermo-mechanical, and rolling contact problems, are discussed. Rothe's method is used to discretise the problems. After discretisation in time with an adequate time stepping scheme, e. g. the Newmark method, which is studied exemplarily in this article, the semi discrete problems are solved by low order finite elements. The finite element discretisation is based on the solution techniques, which were described in the first part of this series of articles [H. Blum, H. Kleemann, A. Rademacher, A. Schröder: On Solving Frictional Contact Problems, Part I: Abstract Framework and the Static case]. Numerical results, including the application of the presented techniques to an example from production engineering, illustrate the performance of the presented techniques in every considered problem type.

1. Introduction

Dynamic frictional contact problems are an adequate model for many engineering processes, e.g., in milling and grinding processes, vehicle design and ballistics. In all of these processes, the main effects emerge from the contact at the surface of the bodies under consideration. E.g. in grinding processes, the workpiece interacts with the grinding wheel only in a small contact zone. However, the behaviour of the grinding machine is strongly affected by the resulting contact and frictional forces, and the thermal effects. The reliable simulation of such a process has to predict precisely all mentioned effects and their influence onto the whole body.

In this article, an appropriate discretisation scheme for dynamic contact problems involving frictional, thermal, and rotational effects is developed. The discretisation scheme is based on Rothe's method to discretise time dependent problems. The discretisation is carried out in two steps. First, the problem is discretised in time by an appropriate time stepping scheme. Here, we use finite difference schemes, like the Newmark [23] or the Generalized-α [10] method. The temporal discretisation of dynamic contact problems is a difficult task. Several approaches based on different problem formulations have been presented in literature. Techniques for smoothing and stabilizing the computation with special finite elements, e.g. Mortar finite elements, are presented in [15, 21, 25]. The Newmark scheme, which is extended by an additional L^2-projection for stabilisation, is used in [13]. In [17, 18], a time stepping schme is introduced, which is based on the additive splitting of the acceleration into two parts, representing the interior and the contact forces. Algorithms for dynamic contact/impact problems are derived in [1, 20]. They are based on the conservation of energy and momentum. Special contact elements in combination with Lagrange multipliers are presented in [2]. The penalty method is used in [30] to solve the discrete problems. The approach, which is used here, was developed in [12, 26, 27]. It is based on variational inequalities and optimization algorithms. A detailed survey of this topic can be found in the monographs [19, 29]. Especially in [29], all mentioned problem types are introduced and discussed.

From the discretisation in time, a sequence of problems arises, which are continuous in space and discrete in time. These problems are called semi discrete. They have the same mathematical structure as static contact problems. Consequently, the same solution techniques can be applied. In the first part of this series of articles [5], an approach to solve static frictional contact problems numerically has been presented. At first, the equivalence of several problem formulations, the

Key words and phrases. Frictional Contact problems, Signorini problem, Coulomb friction, Thermo-mechanical contact, Finite element method, Optimization.

[1] Institute of Applied Mathematics, Technische Universität Dortmund, Vogelpothsweg 87, 44227 Dortmund, Germany.

[2] Department of Mathematics, Humbold-Universität zu Berlin, Unter den Linden 6, 10099 Berlin, Germany.

strong formulation, the weak formulation as variational inequality, the mixed formulation, and the formulation as minimisation problem, is discussed. It is shown that the mixed formulation is favourable as starting point for the discretisation, for which a stable mixed finite element method is used. The arising discrete problems are solved by building the Schur complement and applying quadratic optimization techniques. The assets and drawbacks of this method compared to other solution techniques known from literature are discussed. Here, we rewrite the semi discrete variational inequalities as mixed problems and use a mixed finite element solution approach. Only small modifications on the static solution algorithms are necessary.

The article is organised as follows: In the next section, dynamic Signorini and obstacle problems without friction including damping effects are discussed. Based on the continuous problem formulation, the discretisation is presented. Numerical results illustrate the properties of the solution algorithm. In Section 3, the problem formulation is extended by frictional effects. Furthermore, the necessary modifications of the discretisation are discussed. The coupling between friction and heat is the focus of Section 4. Thermal effects are included in the problem formulation and the discretisation scheme. Rotational effects are discussed in Section 5. They are introduced in the discratisation scheme by an arbitrary Lagrangian Eulerian (ALE) ansatz. The approach is applied on an example from production engineering, where a damped thermomechanical contact problem involving rotational effects occurs. The article concludes with a discussion of the results.

2. Dynamic Signorini and Obstacle Problems

Dynamic contact problems without friction, namely dynamic Signorini and obstacle problems, are the topic of this section. This is an extension of section 3.2 in [5], where static Signorini and obstacle problems are considered, by inertia terms. Furthermore, viscous damping is included in the problem formulation. The presented continuous formulation and discretisation technique are the basis for all following problems.

2.1. Continuous Formulation.

The strong and the weak formulation of the dynamic Signorini problem are presented. Let $\Omega \subset \mathbb{R}^3$ be the basic domain and $I := [0,T] \subset \mathbb{R}$ a time interval. The boundary $\partial\Omega$ of Ω is divided into three mutually disjoint parts Γ_D, Γ_C and Γ_N with positive measure. Homogeneous Dirichlet and Neumann boundary conditions are prescribed on the closed set Γ_D and on Γ_N, respectively. Contact may take place on the sufficiently smooth set Γ_C, $\bar{\Gamma}_C \subset \complement\Gamma_D$. See, e.g., [5], Section 3.2 for more details.

We assume a linear elastic material model with small deformations. The linearized strain operator is given by $\varepsilon(u) := \frac{1}{2}\left(\nabla u + \nabla u^T\right)$, where ∇u is the gradient of the displacement u in space direction. The first and second time derivatives are denoted by $\dot{u}$ and $\ddot{u}$, respectively. The stress operator of linear elasticity, which is defined by the modulus of elasticity E and by Poisson's number ν, is $\sigma(u)$. The density of the material is given by ρ.

For the description of the contact conditions, the techniques presented in [5] are used. The time dependent sufficiently smooth gap function is denoted by g. The displacement on the boundary in normal direction is given by $\delta_n(u)$ and $\sigma_{nn}(u)$ is the stress in normal direction on the boundary. Here, the restriction $\delta_n(u) \leq g$ on Γ_C is considered, $\delta_n(u) \geq g$ can be treated analogously.

We assume that the damping is proportional to the velocity and use the approach of Rayleigh to describe this proportionality. The damping effects are splitted into a mass proportional and a stiffness proportional part. The term $a_d\rho\dot{u}$ reprensents the mass depending damping, where a_d is some positive constant. The stiffness porportional part is given by $\sigma(u) = \sigma\left(u + b_d\dot{u}\right)$ with a constant $b_d \geq 0$.

The initial displacement u_s is in $H^1\left(\Omega,\Gamma_D\right)^3 := \left\{ v \in H^1\left(\Omega\right)^3 \middle| \gamma_{|\Gamma_D}(v) = 0 \right\}$ and the initial velocity v_s is in $L^2\left(\Omega\right)^3$. Here, γ denotes the trace operator of functions in $H^1\left(\Omega,\Gamma_d\right)^3$ onto the boundary $\partial\Omega$. See, e.g., [14] for more details. In what follows, all relations have to be understood almost everywhere.

We choose the unconstrained trial space

$$V := W^{2,\infty}\left(I; L^2\left(\Omega\right)^3\right) \cap L^\infty\left(I; H^1\left(\Omega,\Gamma_D\right)^3\right)$$

for notational convenience, although the existence of a solution in V can not be proven, even in the contact free case [14]. The set of admissible displacements is

$$K := \{\varphi \in V \,|\delta_n(\varphi) \leq g \text{ on } \Gamma_C \times I\}.$$

The L^2-scalar product is defined by $(u,v) = \int_\Omega uv\,dx$ for $u, v \in L^2(\Omega)^3$. Eventually, if the solution u is sufficiently smooth, the strong formulation of the dynamic Signorini problem reads

$$\begin{aligned}
\rho\ddot{u} + a_d\rho\dot{u} - \operatorname{div}(\sigma(u + b_d\dot{u})) &= f && \text{in } \Omega \times I \\
u &= 0 && \text{on } \Gamma_D \times I \\
\sigma_{nn}(u) &= 0 && \text{on } \Gamma_N \times I \\
\delta_n(u) - g &\leq 0 && \text{on } \Gamma_C \times I \\
\sigma_{nn}(u) &\geq 0 && \text{on } \Gamma_C \times I \\
\sigma_{nn}(u)(\delta_n(u) - g) &= 0 && \text{on } \Gamma_C \times I.
\end{aligned}$$

Using integration by parts in space, we obtain the weak formulation

Problem 2.1. Find a function $u \in K$ with $u(t=0) = u_s$ and $\dot{u}(t=0) = v_s$ for which

$$\begin{aligned}
&(\rho\ddot{u}(t) + a_d\rho\dot{u}(t), \varphi(t) - u(t)) + (\sigma(u(t) + b_d\dot{u}(t)), \varepsilon(\varphi(t) - u(t))) \\
\geq\ & (f(t), \varphi(t) - u(t))
\end{aligned}$$

holds for all $\varphi \in K$ and all $t \in I$.

Throughout this article, we assume $f \in L^\infty\left(I; L^2(\Omega)\right)$. A detailed derivation of the weak formulation can be found in [24].

2.2. **Discretisation.** We use Rothe's method to discretise the dynamic Signorini problem. First, the problem is discretised in temporal direction by the Newmark method (see [23]). The resulting spatial problems are approximately solved by low order finite elements. Alternative time stepping schemes are the Generalized-α method, which was examined in [11, 26], and Galerkin space-time methods, which were developed in [4].

2.2.1. *Temporal Discretization.* The time interval I is split into N equidistant subintervals $I_n := (t_{n-1}, t_n]$ of length $k = t_n - t_{n-1}$ with $0 =: t_0 < t_1 < \ldots < t_{N-1} < t_N := T$. The value of a function w at a time instance t_n is approximated by w^n. We use the notation $v = \dot{u}$ and $a = \ddot{u}$ for the velocity and the acceleration, respectively.

In the Newmark method, v and a are approximated as:

$$a^n = \frac{1}{\beta k^2}\left(u^n - u^{n-1}\right) - \frac{1}{\beta k}v^{n-1} - \left(\frac{1}{2\beta} - 1\right)a^{n-1} \tag{2.1}$$

$$v^n = v^{n-1} + k\left[(1-\alpha)\,a^{n-1} + \alpha a^n\right] \tag{2.2}$$

Here, α and β are free parameters in the interval $[0,2]$. For second order convergence, $\alpha = \frac{1}{2}$ is required. Furthermore, the inequality $2\beta \geq \alpha \geq \frac{1}{2}$ has to be valid for unconditional stability (see [16]). For dynamic contact problems, the choice $\alpha = \beta = \frac{1}{2}$ is recommanded to guarantee conservation of energy and momentum (see [2, 26]). For starting the Newmark method the initial acceleration a_s is needed. It can be calculated on the basis of the inital displacement and velocity (see [16]). The semi discrete problem then reads as follows:

Problem 2.2. Find u with $u^0 = u_s$, $v^0 = v_s$ and $a^0 = a_s$, such that in every time step $n \in \{1, 2, \ldots, N\}$, the function $u^n \in K^n$ is the solution of the variational inequality

$$(\rho a^n + a_d\rho v^n, \varphi - u^n) + (\sigma(u^n + b_d v^n), \varepsilon(\varphi - u^n)) \geq (f(t_n), \varphi - u^n) \tag{2.3}$$

for all $\varphi \in K^n$. Moreover u^n, v^n and a^n have to fulfill the equations (2.1) and (2.2).

The set $K^n := \left\{ \varphi \in H^1(\Omega, \Gamma_D)^3 \,|\delta_n(\varphi) \leq g^n \text{ on } \Omega \right\}$ is the time discretized set of admissible displacements. Substituting the equation (2.1) with $\alpha = \beta = \frac{1}{2}$ in the inequality (2.3) leads to

$$\begin{aligned} & \left(1 + \frac{1}{2}ka_d\right)(\rho u^n, \varphi - u^n) + \frac{1}{2}k(k + b_d)(\sigma(u^n), \varepsilon(\varphi - u^n)) \\ \geq & \left(\frac{1}{2}k^2 f(t_n) + \rho\left(1 + \frac{1}{2}ka_d\right)u^{n-1} + k\,\rho v^{n-1} - \frac{1}{4}k^3 a_d \rho a^{n-1}, \varphi - u^n\right) \\ & + \frac{1}{2}kb_d\left(\sigma\left(u^{n-1} - \frac{1}{2}k^2 a^{n-1}\right), \varepsilon(\varphi - u^n)\right). \end{aligned}$$

This can be written as

$$c(u^n, \varphi - u^n) \geq (F_1^n, \varphi - u^n) + (\sigma(F_2^n), \varepsilon(\varphi - u^n)), \tag{2.4}$$

where c is defined by

$$c(\omega, \varphi) := \left(1 + \frac{1}{2}ka_d\right)(\rho\omega, \varphi) + \frac{1}{2}k(k + b_d)(\sigma(\omega), \varepsilon(\varphi)),$$

F_1^n by

$$F_1^n := \frac{1}{2}k^2 f(t_n) + \rho\left(1 + \frac{1}{2}ka_d\right)u^{n-1} + k\,\rho v^{n-1} - \frac{1}{4}k^3 a_d \rho a^{n-1}$$

and F_2^n by

$$F_2^n := \frac{1}{2}kb_d\left(u^{n-1} - \frac{1}{2}k^2 a^{n-1}\right).$$

The bilinearform c is uniformly elliptic, continuous and symmetric. Thus, an elliptic variational inequality has to be solved in each time step. For solving the inequality (2.4), the techniques presented in [5] can directly be applied. We give here only a brief overview and refer to [5] for the details. An efficient way for solving variational inequalities is given by their mixed formulation, where the Lagrange multipliers may be interpreted as contact forces. We obtain the equivalent mixed problem formulation

Problem 2.3. Find (u, λ) with $u^0 = u_s$, $v^0 = v_s$ and $a^0 = a_s$, such that $(u^n, \lambda^n) \in V^n \times \Lambda^n$ is the solution of the system

$$c(u^n, \varphi) + \langle \lambda^n, \delta_n(\varphi) \rangle = (F_1^n, \varphi - u^n) + (\sigma(F_2^n), \varepsilon(\varphi - u^n)) \tag{2.5}$$

$$\langle \mu - \lambda^n, \delta_n(u^n) - g^n \rangle \leq 0 \tag{2.6}$$

for all $\varphi \in V^n$, all $\mu \in \Lambda^n$ and all $n \in \{1, 2, \ldots, N\}$. Based on the equations (2.1) and (2.2), the functions v^n and a^n are calculated in a postproceesing step.

Here, Λ^n is the dual cone of the set $G^n := \left\{ \mu \in H^{1/2}(\Gamma_C) \middle| \, \mu \leq 0 \right\}$. The dual pairing is expressed by $\langle \cdot, \cdot \rangle$. The set $V^n := H^1(\Omega, \Gamma_D)$ is the time discretised unconstrained trial space.

2.2.2. *Spatial Discretisation.* A finite element approach is applied to discretise the mixed problem 2.3. The trial spaces are V_h and Λ_H. Trilinear basis functions on the mesh $\mathbb{T}$ are used for the finite element space V_h. The discrete Lagrange multipliers are piecewise constant and are contained in the set Λ_H. The index H indicates, that coarser meshes may be chosen for the Lagrange multipliers. In our calculations, we use $H = 2h$ for stability reasons. The space and time discrete problem is

Problem 2.4. Find $(u_h^n, \lambda_H^n) \in V_h \times \Lambda_H$ with $u_h^0 = I_h u_s$, $v_h^0 = I_h v_s$ and $a_h^0 = I_h a_s$, such that the system

$$c(u_h^n, \varphi_h) + \langle \lambda_H^n, \delta_n(\varphi_h) \rangle = \left(F_{1,h}^n, \varphi - u^n\right) + \left(\sigma\left(F_{2,h}^n\right), \varepsilon(\varphi - u^n)\right) \tag{2.7}$$

$$\langle \mu_H - \lambda_H^n, \delta_n(u_h^n) - g^n \rangle \leq 0 \tag{2.8}$$

is valid for all $\varphi_h \in V_h$, all $\mu_H \in \Lambda_H$ and all $n \in \{1, 2, \ldots, N\}$. Additionally, the equations (2.1) and (2.2) determine v_h^n and a_h^n.

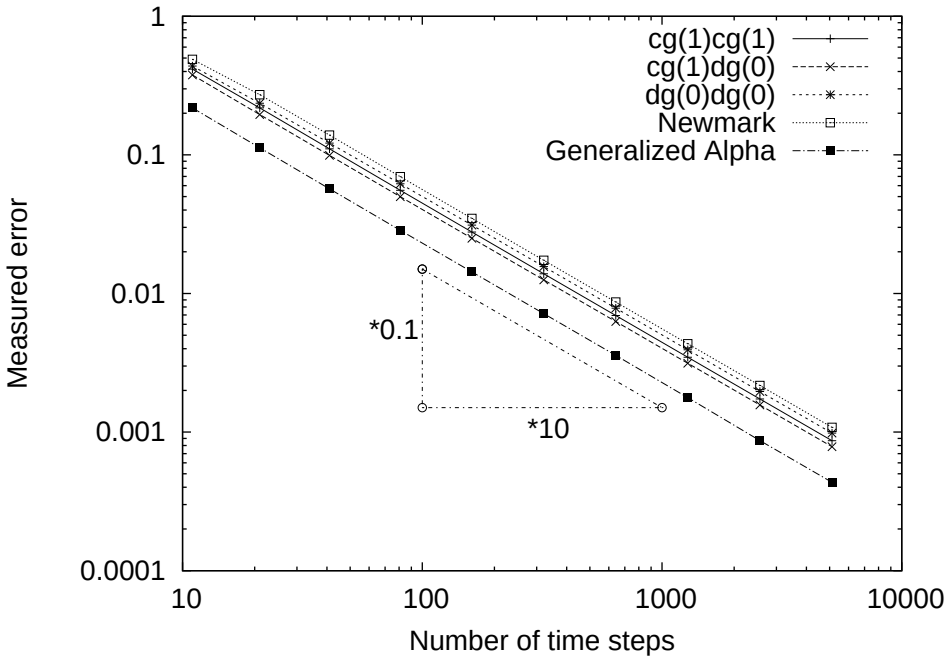

FIGURE 2.1. Convergence rate w.r.t. k for different time stepping schemes

Here, $F^n_{1,h}$ is given by

$$F^n_{1,h} := \frac{1}{2}k^2 f(t_n) + \rho\left(1 + \frac{1}{2}ka_d\right)u^{n-1}_h + k\,\rho v^{n-1}_h - \frac{1}{4}k^3 a_d \rho a^{n-1}_h$$

and $F^n_{2,h}$ by

$$F^n_{2,h} := \frac{1}{2}kb_d\left(u^{n-1}_h - \frac{1}{2}k^2 a^{n-1}_h\right).$$

The prefix I_h denotes the L^2-projection of a function onto V_h.

2.3. **Numerical Examples.** We will investigate three examples for dynamic contact problems. The first one is an obstacle problem without damping. Then, a 2D linear elastic Signorini problem without and with damping is considered.

2.3.1. *Obstacle Problem.* The main difference between obstacle and Signorini problems lies in the description of the contact conditions. In Signorini problems, the contact occurs on the boundary. In obstacle problems, however, the contact occurs in the interior of the domain. Thus, the set of admissible displacements is given by $K = \{\varphi \in V \,|\varphi \geq \psi \text{ on } \Omega \times I\}$. In what follows, a 1d example, whose results are almost the same as for the analogous 2d example (see [26]), is examined. It holds $\Omega = I = [0,1]$, $f = 0$, $u_s(x) = \sin(\pi x)$, $v_s \equiv 0$ and $a_d = b_d = 0$. The obstacle is given by $\psi \equiv 0$. The analytical solution of this problem is $u(x,t) = \sin(\pi x)\,|\cos(\pi t)|$.

The convergence rates for the Newmark-, the Genralized-α-, the $cg(1)cg(1)$-, the $cg(1)dg(0)$- and the $dg(0)dg(0)$ method are shown in Figure 2.1. An uniform mesh width of $h = 2^{-11}$ is choosen in these calculations and the error is measured in the $L^\infty\left(I; L^2(\Omega)\right)$ norm. The results are similar for all methods. They all converge of first order. For the $cg(1)dg(0)$- and the $dg(0)dg(0)$ method, this is expected. But the other methods converge normally of second order. But here, the solution is not regular enough because of the modules in it. It must be mentioned, that the results of the Generalized-α methods are only satisfactory in this special case. In the general case, it is impossible to obtain reasonable results with the Generalized-α method for dynamic obstacle problems (see [26]).

2.3.2. *Cantilever Beam.* As a 2D example for a Signorini problem, we consider a cantilever beam in frictionless contact with a flat rigid surface. The length of the beam is $l = 0.2\,\mathrm{m}$ and the height is $h = 0.05\,\mathrm{m}$. The domain Ω is given by $\Omega = [0, 0.05] \times [0, 0.2]$. The material parameters of the linear elastic plain strain material law are $E = 73 \cdot 10^9\,\mathrm{Pa}$ and $\nu = 0.3$, which corresponds to aluminium. The density is $\rho = 2770\,\mathrm{kg/m^2}$. The beam is fixed on the

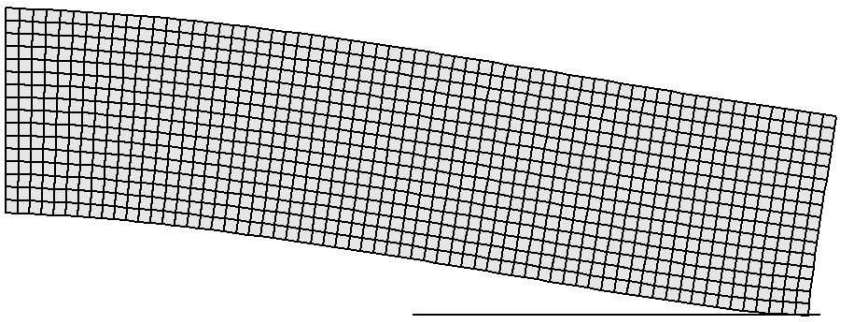

FIGURE 2.2. Geometry of the cantilever beam (displacements scaled by a factor of 5)

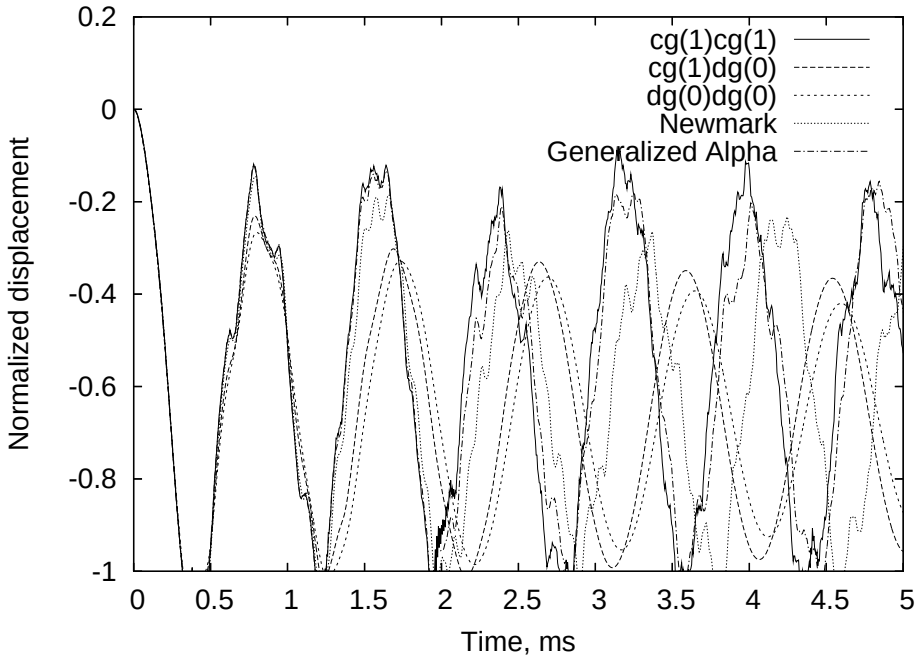

FIGURE 2.3. Normalized displacement at the tip of the beam

set $\Gamma_D = \{(x,y)x \in \partial\Omega |\, y = 0\}$. Inhomogeneous Neumann boundary conditions are assumed on $\Gamma_N = \{(x,y) \in \partial\Omega |\, x = 0 \wedge 0.15 \leq y \leq 0.2\}$. The surface traction on Γ_N is $q = 1.25 \cdot 10^5\,\mathrm{N/m}$. The possible contact zone Γ_C is given by $\Gamma_C = \{(x,y) \in \partial\Omega |\, x = 0.05 \wedge 0.1 \leq y \leq 0.2\}$. The gap between the beam and the rigid surface is choosen as $g = 2.5 \cdot 10^{-5}\,\mathrm{m}$, which is approximately the maximal deflection in the unconstrained case. The geometry of this example is shown in Figure 2.2. The initial displacement and the initial velocity are zero. Here, we choose $a_d = b_d = 0$. The time interval is choosen as $I = \left[0, 5 \cdot 10^{-3}\right]$. The length of the time step is $k = 5 \cdot 10^{-6}\,\mathrm{s}$. We use 4096 quads to discretise the domain Ω. In Figure 2.3, the normalized displacement at the point $A = (0.05, 0.2)$, which corresponds to the tip of the beam, is depicted for different time stepping schemes. The results for the $cg(1)cg(1)$-, Newmark- and Generalized-α method are similar. One gets a somehow periodic response, what is expected from the physical point of view. Furthermore, since no damping is assumed, the amplitude should stay constant. The only difference between the methods is in the length of the period. The $cg(1)dg(0)$- and the $dg(0)dg(0)$ lead to a smoother and lower reponse because of their damping properties. The results are exemplary for the behaviour of the time stepping methods. In what follows, we will only show the results for the Newmark method. The results of the other methods behave in the same way as in this example compared with the results for the Newmark method.

Now, damping effects are included. We choose the damping parameters $a_d = b_d = 5 \cdot 10^{-6}$. In Figure 2.4, the normalized displacement of the cantilever beam with and without damping is compared. The damped response is smoother and the amplitude is decaying. In particular, the damped beam hits the surface only two times. Then it vibrates free, which is expected from the

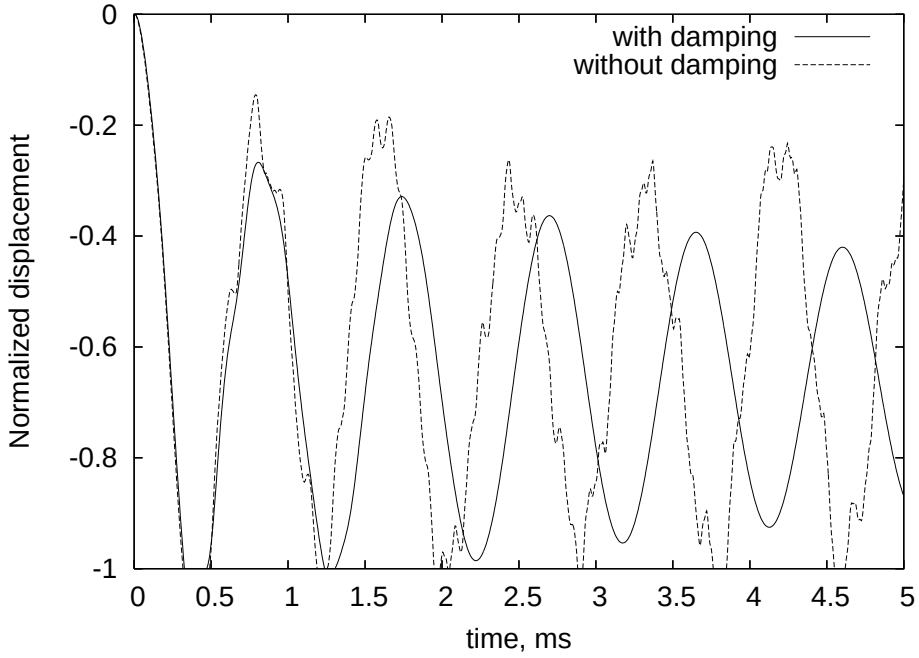

FIGURE 2.4. Normalized displacement for the Newmark method with and without damping

physical point of view. To ease the notation, damping is not included in the following problem formulations, although the inclusion is easy to realise.

3. Dynamic Signorini Problems with Friction

We extend the problems considered in the previous section by frictional effects now. In contrast to static friction problems, which are presented in [5], the frictional constraint is applied on the velocity and not on the displacement. Nevertheless, the same solution techniques as in the static case can be used after discretisation in temporal direction.

3.1. **Continuous Problem Formulation.** In this section the strong and the weak formulation of the dynamic Signorini problem with friction are presented. We extend the formulation described in section 2.1 here. The displacement on the boundary in tangential direction is denoted by $\delta_t(u)$ and the tangential stress by $\sigma_{nt}(u)$. As in the static case, the tangential contact stresses are bounded by the frictional resistance s. However, no constraints are prescribed on the tangential displacement, but on the tangetial velocity.

If the solution is sufficiently smooth, we obtain the strong formulation

$$\begin{aligned}
\rho\ddot{u} - \operatorname{div}(\sigma(u)) &= f && \text{in } \Omega \times I \\
u &= 0 && \text{on } \Gamma_D \times I \\
\sigma_{nn}(u) &= 0 && \text{on } \Gamma_N \times I \\
\delta_n(u) - g &\leq 0 && \text{on } \Gamma_C \times I \\
\sigma_{nn}(u) &\geq 0 && \text{on } \Gamma_C \times I \\
\sigma_{nn}(u)\,(\delta_n(u) - g) &= 0 && \text{on } \Gamma_C \times I \\
|\sigma_{nt}(u)| &\leq s && \text{on } \Gamma_C \times I \\
|\sigma_{nt}(u)| &< s && \Rightarrow \delta_t(\dot{u}) = 0 \\
|\sigma_{nt}(u)| &= s && \Rightarrow \exists \zeta \in \mathbb{R}_{\geq 0} : \delta_t(\dot{u}) = \zeta \sigma_{nt}.
\end{aligned}$$

The weak formulation of the dynamic Signorini problem with friction, see e.g. [12], reads

Problem 3.1. Find a function $u \in K$ with $u(t=0) = u_s$ and $\dot{u}(t=0) = v_s$ for which

$$\begin{aligned}
&(\rho\ddot{u}(t), \dot{\varphi}(t) - \dot{u}(t)) + (\sigma(u(t)), \varepsilon(\dot{\varphi}(t) - \dot{u}(t))) + j(\dot{\varphi}(t)) - j(\dot{u}) \\
\geq\ & (f(t), \dot{\varphi}(t) - \dot{u}(t))
\end{aligned}$$

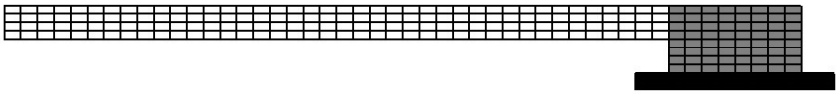

FIGURE 3.1. Finite element mesh of the spring-mass system

holds for all $\varphi \in K$ and all $t \in I$.

The frictional resistance is represented by the non-differentiable functional $j(\varphi) := (s, |\delta_t(\varphi)|)_{\Gamma_C}$, where $s(t,x) \geq 0$ is assumed to be contained in $L^\infty\left(I; L^2\left(\Gamma_C\right)\right)$. In what follows, we use the Coulomb friction law to specify the function s, i. e., we choose $s = \mathcal{F}\,|\sigma_{nn}(u)|$, where $\mathcal{F} \geq 0$ denotes the coefficient of friction.

3.2. **Discretisation.** The discretisation of the dynamic Signorini problem with friction is carried out in the same way as for the frictionless case, wich was described in section 2.2. We end up with the following semi discrete problem in mixed form:

Problem 3.2. Find $(u, \lambda_n, \lambda_t)$ with $u^0 = u_s$, $v^0 = v_s$ and $a^0 = a_s$, such that $(u^n, \lambda_n^n, \lambda_t) \in V^n \times \Lambda_n^n \times \Lambda_t^n$ is the solution of the system

$$\begin{aligned} c(u^n, \varphi) + \langle \lambda_n^n, \delta_n(\varphi)\rangle + \langle \lambda_t^n, \delta_t(\varphi)\rangle &= (F^n, \varphi) \\ \langle \mu_n - \lambda_n^n, \delta_n(u^n) - g^n\rangle & \\ + \frac{1}{k}\langle \mu_t - \lambda_t^n, \delta_t(u^n) - r^n\rangle &\leq 0 \end{aligned}$$

for all $\varphi \in V^n$, all $\mu_n \in \Lambda_n^n$, all $\mu_t \in \Lambda_t^n$ and all $n \in \{1, 2, \ldots, N\}$. Based on the equations (2.1) and (2.2), the functions v^n and a^n are calculated in a postproceesing step.

Here, Λ_t^n is the dual cone of the set G^n. The function $r^n := \delta_t\left(u^{n-1} - \frac{1}{2}k^2 a^{n-1}\right)$ is based on the equations (2.1) and (2.2) with

$$\delta_t(v^n) = \frac{1}{k}\left(\delta_t(u^n) - r^n\right).$$

Using the techniques described in [5], Problem 3.2 can be solved approximately. The only difference is the additional term r^n, which is constant throughout the solution process in each time step.

3.3. **Numerical Example.** Our model example for frictional contact is a spring-mass system, where the mass is in frictional contact with a rigid surface. The spring is modeled by an elastic rod of length $l_1 = 2.0\,\mathrm{m}$ and height $h_1 = 0.2\,\mathrm{m}$. The following material properties are assumed in a plain strain linear elastic material model: $E_1 = 10^3\,\mathrm{Pa}$, $\nu_1 = 0$ and $\rho_1 = 0.01\,\mathrm{kg/m^2}$. The mass is given by a rectangular block of length $l_2 = 0.4\,\mathrm{m}$ and height $h_2 = 0.4\,\mathrm{m}$ with the matrial parameters $E_2 = 10^9\,\mathrm{Pa}$, $\nu_2 = 0$ and $\rho_2 = 2.5\,\mathrm{kg/m^2}$. By selecting $\rho_1 \ll \rho_2$ and $E_2 \gg E_1$, we gain a nearly weightless and flexible spring and an approximately rigid mass. The finite element mesh is depicted in Figure 3.1, where the spring, the mass and the rigid foundation have different colours. The domain Ω is given by

$$\Omega = [0, 2.0] \times [-0.2, 0] \cup [2.0, 2.4] \times [-0.4, 0].$$

The time interval I is $[0, 3]$. The spring is fixed at the left end, i.e. homogeneous Dirichlet boundary conditions are assumed on $\Gamma_{D_1} = \{(x,y) \in \partial\Omega \,|\, x = 0\}$. Furthermore, the displacement in y direction on $\Gamma_{D_2} = \{(x,y) \in \partial\Omega \,|\, y = 0\}$ is constrained. A constant normal stress of $q_1 = 15\,\mathrm{N/m}$ is applied on $\Gamma_N = \{(x,y) \in \partial\Omega \,|\, x = 2.4 \wedge 0 \geq y \geq -0.2\}$. The set $\Gamma_C = \{(x,y) \in \partial\Omega \,|\, y = -0.4\}$ is the possible contact set. The point A, in which we will observe the displacement and the velocity, is given by $A = (2.4, -0.1)$. We use 14336 quads to discretise Ω. The time step length is selected as $k = 0.001$. The gap is choosen as $g = -10^{-10}m$. Since the mass is modelled nearly rigid and cannot move up, this results in a high contact stress. The friction coefficent is choosen as $\mathcal{F} = 0.125$. The tolerance of the fixpoint method in the solver is set to 10^{-13}. It has been achieved in $1 - 10$ iterations, where the number of iterations was decreasing with growing t.

In Figure 3.2, the results with and without friction are presented. The displacement in the point A is compared in Figure 3.2(a). In the frictionless case, the displacement is a sinusoidal

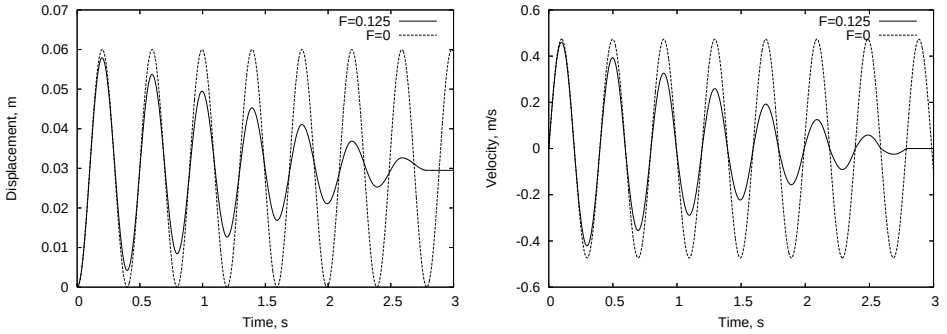

(a) Displacement

(b) Velocity

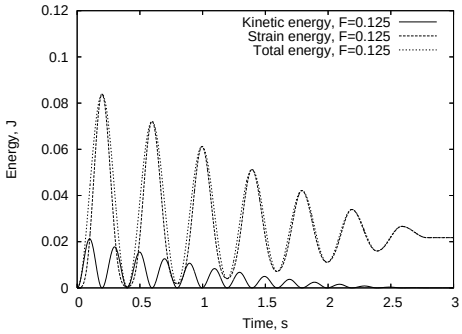

(c) Energy with friction

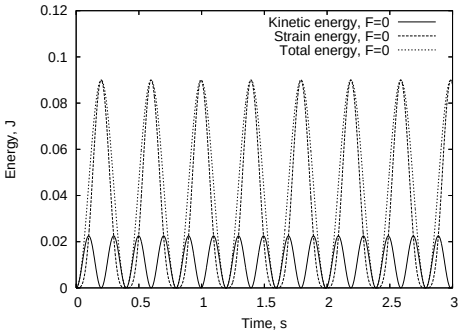

(d) Energy without friction

FIGURE 3.2. Comparison of displacement, velocity and energy with and without friction for the spring-mass system with Coulomb friction

vibration. In the frictional case, however, the frequence of the oscillation is the same, but the amplitude is decaying as expected. The corresponding results for the velocity are shown in Figure 3.2(b). The energy is compared in the Figures 3.2(c) and 3.2(d). In the frictional case, the kinetic energy decays to zero and the strain energy attains a fixed value, when the movement stops. In the frictionless case, the energy is oscilatting in agreement with the diplacement and the velocity of the spring-mass system. All numerical results meet the physical expectations.

4. Dynamic Thermo-Mechanical Contact Problems

During frictional contact, energy is dissipated. A portion of this energy generates heat, which is induced into the participating bodies. In this section, we introduce a model for this physical process and present a numerical solving algorithm based on the techniques presented in the previous sections.

4.1. **Continuous Problem Formulation.**

We introduce the continuous formulation of the model for thermo-mechanical contact. First, we present briefly the linear theory of thermo-elasticity, which describes the effects of heat on an elastic body. A detailed presentation may be found in [9]. Then, the coupling of friction and heat is discussed.

The linear elastic model described in Section 2.1 is extended by thermal effects here. The heat of the body is given by the function $\theta \in V_\theta$ with

$$V_\theta := \left\{ \varphi \in L^2\left(I; H^1(\Omega, \Gamma_D)\right) \middle| \dot{\varphi} \in L^2\left(I; H^{-1}(\Omega)\right) \right\}.$$

We assume for notational simplicity that homogeneous Dirichlet boundary conditions hold on Γ_D for the heat distribution, too. Possibly nonhomogeneous Neumann boundary conditions are prescribed on Γ_C, which are specified by the function $q \in L^2\left(I; L^2(\Gamma_C)\right)$. Homogeneous Neumann boundary conditions are assumed on Γ_N. The inner heat sources are described by the function $l \in L^2\left(I; L^2(\Omega)\right)$. The initial temperature is $\theta_s \in H^1(\Omega, \Gamma_D)$. The specific heat is given by the constant ζ and the constant κ denotes the conductivity. Thus, the heat equation reads:

Problem 4.1. Find a function $\theta \in V_\theta$ with $\theta(0) = \theta_s$, which fulfills the variational equation

$$\left\langle \zeta \dot{\theta}, \varphi \right\rangle + (\kappa \nabla \theta, \nabla \varphi) = (l, \varphi) + (q, \varphi)_{\Gamma_C} \tag{4.1}$$

for all $\varphi \in H^1(\Omega, \Gamma_D)$ and all $t \in I$.

The connection between heat and displacement is mainly governed by the coefficient of thermal expansion α. For a more convenient description, we use the stress-temperature modulus m, which is given by

$$m = -\frac{\alpha E}{1+\nu}\left(\frac{3\nu}{1-2\nu} + 1\right).$$

Due to the temperature, thermal stresses, which are modelled by $m(\theta - \theta_s)\,\mathrm{I}$, occur in the elastic body. In the heat equation, an additional internal heat source due to the elastic deformation has to be included. It is specified by the term $m\theta_s \mathrm{tr}\,\dot{\varepsilon}(u)$.

During the frictional contact, energy is disspated. This energy is transfered mostly into heat. The generated energy is given by

$$\int_I \int_{\Gamma_C} \sigma_{nt} \delta_t(\dot{u})\, dx\, dt.$$

The heat is transfered into the elastic body, the obstacle and the enviroment. We assume that a fixed portion of the generated energy enters the elastic body. The proportionality factor is denoted by $K_W \in [0,1]$. The heat transfer between the obstacle and the rigid foundation in the contact zone is neglected. The generated heat is included in the heat equation as nonhomogeneous Neumann boundary conditions on Γ_C, i.e.

$$q = K_W \sigma_{nt} \delta_t(\dot{u}).$$

Together with the formulation of the frictional contact problem in Section 3.1, the strong formulation of the thermo-elastic contact problem is given by

$$\begin{aligned}
\rho\ddot{u} - \mathrm{div}(\sigma(u) + m(\theta - \theta_s)\,\mathrm{I}) &= f && \text{in } \Omega \times I \\
\zeta\dot{\theta} - \mathrm{div}(\kappa\nabla\theta) + m\theta_0 \mathrm{tr}\dot{\varepsilon}(u) &= l && \text{in } \Omega \times I \\
u = \theta &= 0 && \text{on } \Gamma_D \times I \\
\sigma_{nn}(u) = \frac{\partial\theta}{\partial n} &= 0 && \text{on } \Gamma_N \times I \\
\delta_n(u) - g &\leq 0 && \text{on } \Gamma_C \times I \\
\sigma_{nn}(u) &\geq 0 && \text{on } \Gamma_C \times I \\
\sigma_{nn}(u)(\delta_n(u) - g) &= 0 && \text{on } \Gamma_C \times I \\
|\sigma_{nt}(u)| &\leq s && \text{on } \Gamma_C \times I \\
|\sigma_{nt}(u)| &< s && \Rightarrow \delta_t(\dot{u}) = 0 \\
|\sigma_{nt}(u)| &= s && \Rightarrow \exists \xi \in \mathbb{R}_{\geq 0} : \delta_t(\dot{u}) = \xi\sigma_{nt} \\
\frac{\partial\theta}{\partial n} &= K_W\sigma_{nt}\delta_t(\dot{u}) && \text{on } \Gamma_C \times I,
\end{aligned}$$

if u and θ are sufficiently smooth. The weak formulation reads:

Problem 4.2. Find a function $(u, \theta) \in K \times V_\theta$ with $u(0) = u_s$, $\dot{u}(0) = v_s$ and $\theta(0) = \theta_s$, such that

$$\begin{aligned}
(\rho\ddot{u}, \dot{\varphi} - \dot{u}) + (\sigma(u) + m(\theta - \theta_s)\,\mathrm{I}, \varepsilon(\dot{\varphi} - \dot{u})) & \\
+ j(\dot{\varphi}) - j(\dot{u}) &\geq (f, \dot{\varphi} - \dot{u}) \\
\left\langle \zeta\dot{\theta}, \chi \right\rangle + (\kappa\nabla\theta, \nabla\chi) + (m\theta_s \mathrm{tr}\dot{\varepsilon}(u), \chi) & \\
- (K_W\sigma_{nt}\delta_t(\dot{u}), \chi)_{\Gamma_C} &= (l, \chi)
\end{aligned}$$

holds for all $\varphi \in K$, all $\chi \in V_\theta$ and $t \in I$.

4.2. **Discretisation.** The discretisation of the frictional part of the thermo-elastic contact problem is carried out as described in Section 3.2. Here, we focus on the discretisation of the heat part and on the solution of the discrete system.

For the temporal discretisation of the heat equation, we use the Crank-Nicolson scheme, see, e.g., [16]. The time discretisation of equation (4.1) reads

$$\begin{aligned} & (\zeta\theta^n,\varphi)+\frac{1}{2}k\,(\kappa\nabla\theta^n,\nabla\varphi) \\ = \; & \left(\zeta\theta^{n-1},\varphi\right)+\frac{1}{2}k\left(\kappa\nabla\theta^{n-1},\nabla\varphi\right) \\ & +\frac{1}{2}k\left(l\left(t_n\right)+l\left(t_{n-1}\right),\varphi\right)+\frac{1}{2}k\left(q\left(t_n\right)+q\left(t_{n-1}\right),\varphi\right)_{\Gamma_C}. \end{aligned} \tag{4.2}$$

By introducing the notation

$$\begin{aligned} c_\theta(\omega,\varphi) &:= (\zeta\omega,\varphi)+\frac{1}{2}k\,(\kappa\nabla\omega,\nabla\varphi), \\ w\left(t_{n-\frac{1}{2}}\right) &:= \frac{1}{2}\left(w\left(t_n\right)+w\left(t_{n-1}\right)\right), \\ w^{n-\frac{1}{2}} &:= \frac{1}{2}\left(w^n+w^{n-1}\right), \\ L^n &:= \zeta\theta^{n-1}+kl\left(t_{n-\frac{1}{2}}\right), \end{aligned}$$

equation (4.2) simplifies to

$$c_\theta\left(\theta^n,\varphi\right)=\left(L^n,\varphi\right)+\frac{1}{2}k\left(\kappa\nabla\theta^{n-1},\nabla\varphi\right)+k\left(q\left(t_{n-\frac{1}{2}}\right),\varphi\right)_{\Gamma_C}. \tag{4.3}$$

Using equation (4.3) and Problem 3.2, we can state the time discrete version of Problem 4.2:

Problem 4.3. Find $(u,\lambda_n,\lambda_t,\theta)$ with $u^0=u_s$, $v^0=v_s$, $a^0=a_s$, and $\theta^0=\theta_s$, such that the function $(u^n,\lambda_n^n,\lambda_t^n,\theta^n)\in V^n\times\Lambda_n^n\times\Lambda_t^n\times V_\theta^n$ is the solution of the system

$$c\left(u^n,\theta^n,\varphi\right)+\left\langle\lambda_n^n,\delta_n\left(\varphi\right)\right\rangle+\left\langle\lambda_t^n,\delta_t\left(\varphi\right)\right\rangle = \left(F^n,\varphi\right) \tag{4.4}$$

$$\left\langle\mu_n-\lambda_n^n,\delta_n\left(u^n\right)-g^n\right\rangle+\left\langle\mu_t-\lambda_t^n,\frac{1}{k}\left(\delta_t\left(u^n\right)-r^n\right)\right\rangle \leq 0, \tag{4.5}$$

$$\begin{aligned} & c_\theta\left(\theta^n,v^n,\chi\right)-\frac{K_W}{k}\left(\lambda_t^{n-\frac{1}{2}}v_t^{n-\frac{1}{2}},\chi\right)_{\Gamma_C} \\ & \qquad -\frac{1}{2}k\left(\kappa\nabla\theta^{n-1},\nabla\chi\right) = \left(L^n,\chi\right), \end{aligned} \tag{4.6}$$

for all $\varphi\in V^n$, all $\mu_n\in\Lambda_n^n$, all $\mu_t\in\Lambda_t^n$, all $\chi\in V_\theta^n$, and all $n\in\{1,2,\ldots,N\}$. The approximations v^n and a^n are calculated on the basis of the equations (2.1) and (2.2).

Here, the bilinear forms c and c_θ are defined by

$$\begin{aligned} c\left(\omega,\chi,\varphi\right) &:= (\rho\omega,\varphi)+\frac{1}{2}k^2\left(\sigma(\omega)+m\left(\chi-\theta_s\right)\mathrm{I},\varepsilon(\varphi)\right) \\ c_\theta\left(\omega,\chi,\varphi\right) &:= (\zeta\omega,\varphi)+\frac{1}{2}k\left(\kappa\nabla\omega,\nabla\varphi\right)+\frac{1}{2}k\left(m\theta_s\mathrm{tr}\varepsilon(\chi),\varphi\right). \end{aligned}$$

The term $v_t^{n-\frac{1}{2}}$ is given by

$$v_t^{n-\frac{1}{2}}=\frac{1}{2k}\left(\delta_t\left(u^n\right)-r^n\right)+\delta_t\left(v^{n-1}\right).$$

In many cases, the heat induced by the elastic deformation may be neglected, which simplifies the calculation significantly. The discretisation in space of Problem 4.3 leads to a coupled system, which is solved by a fixpoint method. The fixpoint approach is presented in Algorithm 1. The frictional subproblem in the fourth step of Algorithm 1 is solved with the techniques presented in [5].

Algorithm 1 Fixpoint method for solving the system (4.4)-(4.6)

(1) Assemble all matrices and all vectors with constant values
(2) Set $u_{0,h}^n = u_h^{n-1}$ and $\theta_{0,h}^n = \theta_h^{n-1}$
(3) For $i = 1, 2, 3, \ldots$ do
(4) Solve the system (4.4)-(4.5) with $\theta_{i-1,h}^n$
(5) Assemble the vector $q_{i,h}^n$ using $\lambda_{t,i,H}^n$ and $v_{i,h}^n$
(6) Solve the equation (4.6) with $u_{i,h}^n$ and $q_{i,h}^n$
(7) If $\left\|u_{i,h}^n - u_{i-1,h}^n\right\| + \left\|\theta_{i,h}^n - \theta_{i-1,h}^n\right\| < \text{tol}$ then go to (9)
(8) Go to (4)
(9) Set $u_h^n = u_{i,h}^n$ and $\theta_h^n = \theta_{i,h}^n$ and stop

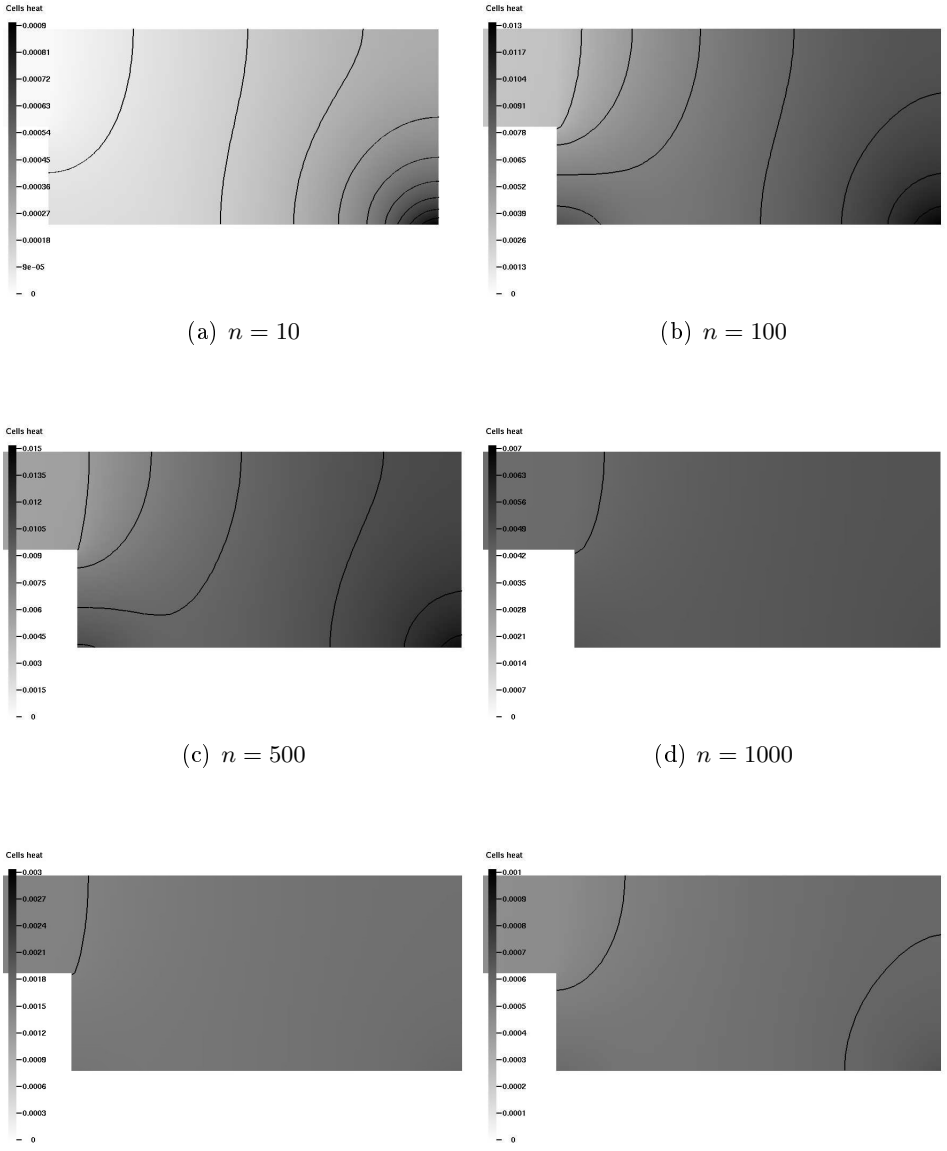

(a) $n = 10$ (b) $n = 100$

(c) $n = 500$ (d) $n = 1000$

(e) $n = 2000$ (f) $n = 2500$

FIGURE 4.1. Heat distribution in the spring-mass system with Coulomb friction

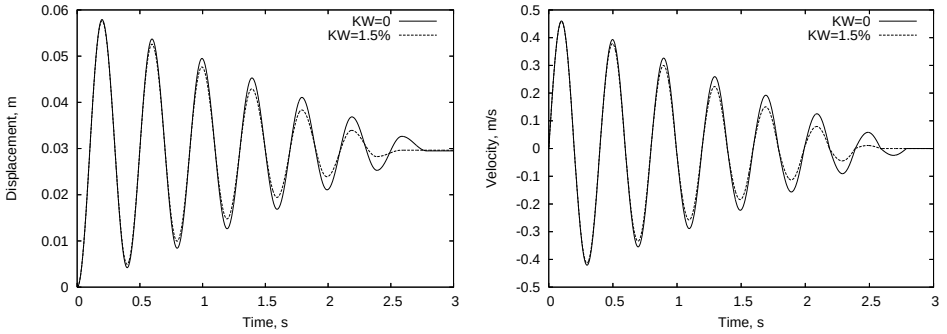

(a) Displacement

(b) Velocity

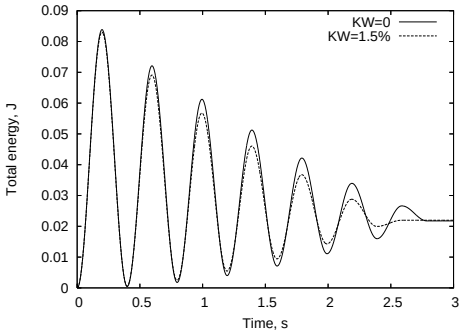

(c) Total Energy

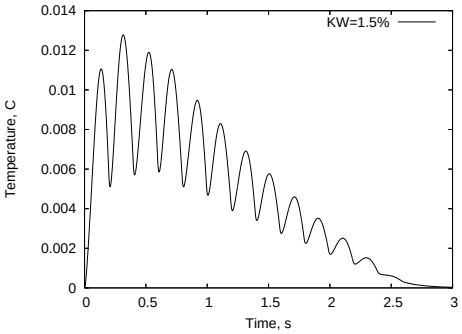

(d) Temperature

FIGURE 4.2. Displacement, velocity, energy and temperature for the spring-mass system with Coulomb friction under consideration of thermal effects

4.3. **Numerical Example.** We examine the same examples as in Section 3.3. In addition, we have to specify the problem data for the heat part. The start temperature θ_s is selected as zero. Homogeneous Dirichlet boundary values are assumed on Γ_D. On $\partial\Omega\backslash(\Gamma_D \cup \Gamma_C)$, homogeneous Neumann boundary conditions are selected. Nonhomogeneous Neumann boundary conditions, which depend on the friction force and on the tangential velocity, are given from the described model on Γ_C. The specific heat of the spring is $\zeta = 10^{-3}\,\frac{\mathrm{m}}{\mathrm{s^2K}}$ and the conductivity is $\kappa = 10^{-2}\,\frac{\mathrm{kg\,m}}{\mathrm{s^3K}}$. For the mass, we assume $\zeta = 10^{-4}\,\frac{\mathrm{m}}{\mathrm{s^2K}}$ and $\kappa = 10^{-3}\,\frac{\mathrm{kg\,m}}{\mathrm{s^3K}}$. In all heat coupled calculations, we select $K_W = 1.5\%$. The coefficient of thermal expansion is $\alpha = 5 \cdot 10^{-8}\,K^{-1}$. The tolerance of the outer fixpoint iteration is selected as 10^{-7}. In this example, $10-20$ iterations are needed to reach the desired tolerance. In Figure 4.1, the heat distribution is presented for different time steps. The maximal temperature is located in the edges of the mass. The maximum moves from the right to the left and back, when the velocity reverses. In Figure 4.2(d), the trend of the temperature over the time interval in the point A is displayed. The temperature is maximal, when the velocity attains is maximum or minimum. This has been expected from the definition of the coupling between friction and temperature. In Figure 4.2(a), the displacement with heat coupling is compared with the displacement without heat coupling. In the case with heat coupling, the amplitude of the displacement decays faster, since the expansion of the mass due to the heating increases the normal force on the surface. The same effect is seen in Figure 4.2(b) and (c), where the velocity and the total energy is compared.

5. Rolling Contact

The inclusion of rotational effects in dynamic contact problems is a difficult task, because the describtion of the contact geometry has to consider the rotation. Especially, if a finer mesh in the contact zone is used, the mesh has to be changed accordingly to the rotational speed. One possibility to overcome this difficulties is to use an ALE ansatz. There, three different configurations are distinguished: the reference configuration, the deformed configuration, and an arbitrary configuration. The reference configuration corresponds to the undeformed body. The arbitrary

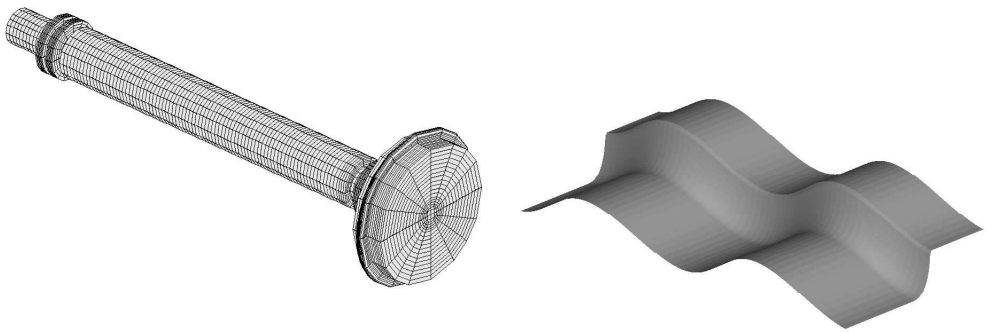

(a) Spindle grinding wheel system (b) Workpiece

FIGURE 5.1. Geometry of the spindle grinding wheel system and of the workpiece

configuration can be specified accordingly to the desired properties of the calculation. A mathematical description of the ALE ansatz would go beyond the scope of this article. Therefor, we give only a general overview and refer for a detailed presentation to [22]. In our calculations, the arbitrary configuration corresponds to the reference configuration, but it rotates with the negative rotational speed of the body. This leads to a fixed configuration for the contact description. Thus, all algorithms presented in this arcticle can be used. Furthermore, the mesh can be be refined in the contact zone and no further changes of the mesh due to the rotation are necessary. The price, we have to pay for the freedom to choose the configuration, is the transport of information, which has to be calculated. We use interpolation for realizing the transport of information. If the rotational speed is constant throughout the calculation, the interpolation can be expressed by matrix vector multiplication, where the matrix does not change during the calculation. The advantage is the small computational effort to realize the interpolation. On the other hand, stability problems can arise under some circumstances.

The ALE ansatz is now illustrated by an example from production engineering. We consider the NC-shape grinding process of free formed surfaces with a toroid grinding wheel. As a subproblem in the simulation of the whole grinding process, dynamic thermo-mechanical problems with damping arise. A detailed survey of the engineering process and the simulation approach is given in [28]. The approach is extended here by considering frictional and thermo-elastic effects. The grinding wheel and the spindle are explicitly included in the finite element analysis. The stiffness of the other parts of the grinding machine are concentrated in elastic bearings. The geometry of the spindle grinding wheel system is depicted in Figure 5.1(a). The length of the spindle is 658 mm, the radius of the grinding wheel is 100 mm, and the radius of the torus is 4.2 mm. This values show the different length scales, which occur in this problem. In particular, the depth of cut is in the range of 0.05 mm to 0.5 mm. The mesh is adaptively refined in the possible contact zone in order to ensure a reasonable resolution of the contact conditions. The mesh, which consists of 27984 cells, is shown in Figure 5.1(a). The problem comprises 88116 unknowns for the elastic part and 29372 unknowns for the heat part, 188 degrees of freedom for the contact and the frictional Lagrange multiplier are created respectively. Homogeneous Dirichlet boundary conditions are assumed on the surface of the bearings. Furthermore, all initial functions are chosen as zero. The modulus of elasticity for the spindle and for the grinding wheel receiver is chosen as $E_1 = 2.1 \cdot 10^{11} \frac{\mathrm{kg}}{\mathrm{m \cdot s^2}}$, for the grinding wheel $E_2 = 2.1 \cdot 10^{13} \frac{\mathrm{kg}}{\mathrm{m \cdot s^2}}$, and for the bearings $E_3 = 10^9 \frac{\mathrm{kg}}{\mathrm{m \cdot s^2}}$ are chosen. The other material parameters are constant throughout the domain and are: $\nu = 0.29$, $\rho = 7.85 \frac{kg}{dm^3}$, $\alpha = 10.8 \cdot 10^{-6}\,\mathrm{K}^{-1}$, $\kappa = 16.7 \frac{\mathrm{kg \cdot m}}{\mathrm{K \cdot s^3}}$, $\zeta = 450 \frac{\mathrm{m^2}}{\mathrm{s^2 \cdot K}}$, $a_d = 0.075$, and $b_d = 0$. The coefficient of friction is chosen as $\mathcal{F} = 0.3$ and the heat distribution coefficient as $K_W = 5\%$. The rotational speed of the grinding wheel is $\omega = 170\pi\,\mathrm{s}^{-1}$. We select $T = 0.02\,\mathrm{s}$ and $k = 10^{-5}\,\mathrm{s}$. The geometry of the workpiece, which has a sinusoidal profile, is presented in Figure 5.1(b), where the vertical and horizontal infeed is chosen as 0.5 mm. The tolerance of the outer fixpoint iteration is chosen as 10^{-8} and of the inner iteration as 10^{-10}.

In Figure 5.2, the displacement in the center of the grinding wheel orthogonal to the plane, in which the workpiece lies, is shown. The sinusoidal profile of the workpiece is carried over to

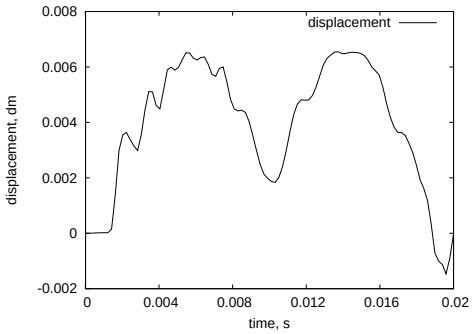

FIGURE 5.2. Displacement in the center of the grinding wheel orthogonal to the workpiece-plane

the displacement of the grinding wheel, as expected. The heat distribution in the contact zone between grinding wheel and workpiece is depicted in Figure 5.3 for different time steps. The effects of the rotation are clear to see. The heat diffuses mainly in the direction of the rotation. Furthermore, the location of the highest temperature moves accordingly to the contact zone. The value of the temperature depends on the tangential stresses and consequently on the normal stresses due to the friction law. This dependence is observed in the heat distribution, e.g., in the middle of the calculation, where the temperature is close to zero, because the grinding wheel is moving down free.

6. Conclusions and Outlook

In this article, the approach for solving static frictional contact problems, which has been presented in [5], has been extended to the dynamic case. We have shown, how the discretisation of dynamic contact problems by Rothe's method leads to semi discrete problems, which have the same structure as static contact problems. Consequently, the same solution techniques are applied successfully. Thermal and rotational effects, which lead to sub-problems of known type, can be considered, too.

The presented discretisation approach is also suited for a posteriori error estimation and adaptive mesh refinement. In [3, 7, 8], results for dynamic Signorini and obstacle problems have been presented. Similar results for the frictional case and for thermo-mechanical problems are being developed.

In the third part of this series of articles [6], static and dynamic two body contact problems with friction are considered. It is shown there, how similar solution techniques can be used to solve two body contact problems, approximately.

Acknowledgement

This research work was supported by the Deutsche Forschungsgemeinschaft (DFG) within the Priority Program 1180, Prediction and Manipulation of Interaction between Structure and Process, and within the Collaborative Research Center 708, 3D-Surface Engineering of Tools for Sheet Metal Forming - Manufacturing, Modelling, Machining.

References

[1] F. Armero and E. Petőcz, *Formulation and analysis of conserving algorithms for frictionless dynamic contact/impact problems*, Comput. Methods Appl. Mech. Engrg., 158 (1998), pp. 269–300.

[2] K. J. Bathe and A. B. Chaudhary, *A solution method for static and dynamic analysis of three-dimensional contact problems with friction*, Computers & Structures, 24 (1986), pp. 855–873.

[3] D. Biermann, H. Blum, T. Janse, A. Rademacher, A. Scheidler, A. Schröder, and K. Weinert, *Space adaptive finite element methods for dynamic signorini problems in the simulation of the nc-shape grinding process*, in Proceedings of 1st International Conference on Process Machine Interaction, Hannover, 2008.

[4] H. Blum, T. Jansen, A. Rademacher, and K. Weinert, *Finite elements in space and time for dynamic contact problems*, Internat. J. Numer. Methods Engrg., to appear (2007).

[5] H. Blum, H. Kleemann, A. Rademacher, and A. Schröder, *On solving frictional contact problems part i: Abstract framework and the static case.* in preparation, 2008.

[6] ———, *On solving frictional contact problems part iii: Two body contact problems.* in preparation, 2008.

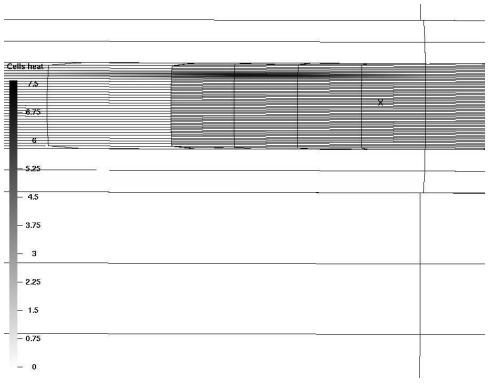

(a) $n = 250$

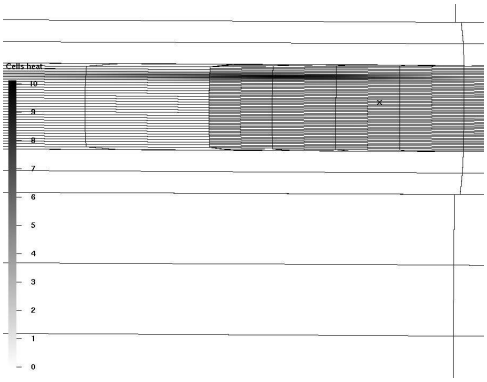

(b) $n = 500$

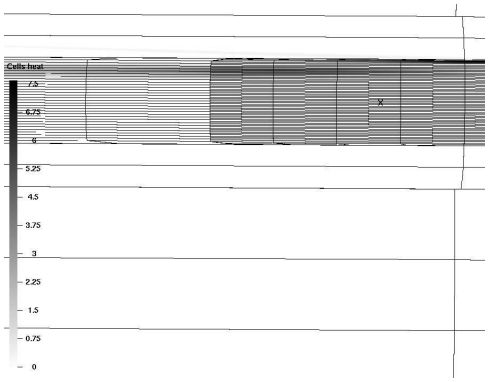

(c) $n = 750$

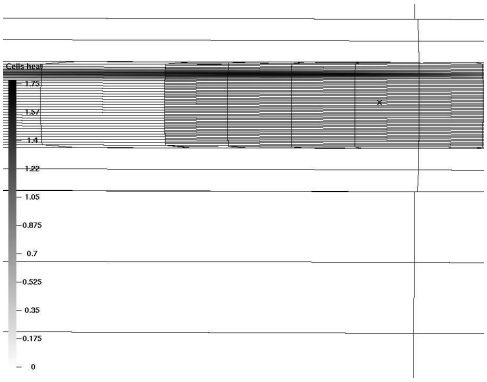

(d) $n = 1000$

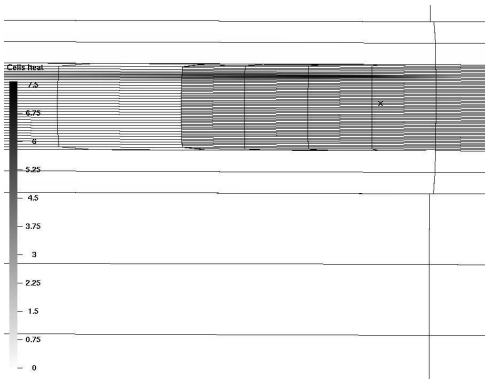

(e) $n = 1250$

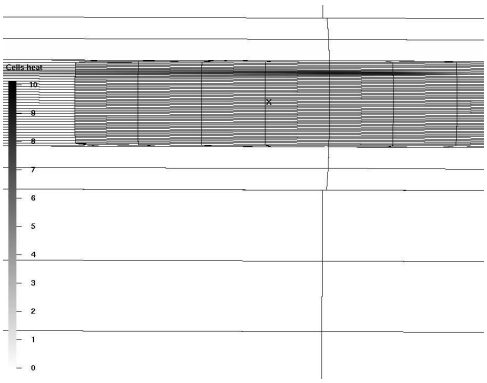

(f) $n = 1500$

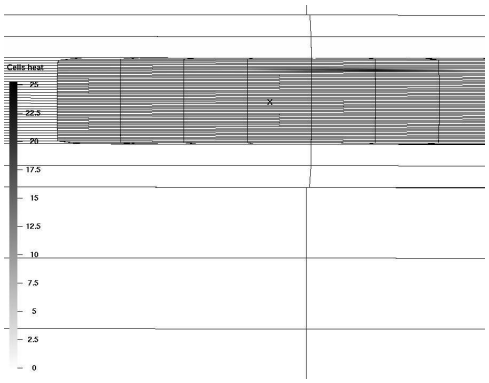

(g) $n = 1750$

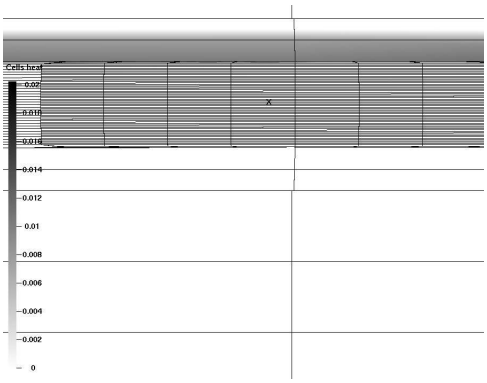

(h) $n = 2000$

FIGURE 5.3. Heat distribution in the contact zone

[7] H. Blum, A. Rademacher, and A. Schröder, *Space adaptive finite element methods for dynamic obstacle problems*, in Proceedings of the 20^{th} Chemnitz FEM Symposium, Chemnitz, 2008.
[8] ———, *Space adaptive finite element methods for dynamic signorini problems*, Computational Mechanics, (2008), p. submitted.
[9] D. E. Carlson, *Linear thermoelasticity*, in Handbuch der Physik, vol. Band VI a/2, Festkörpermechanik II, Springer, Berlin, 1972, pp. 297–346.
[10] J. Chung and G. M. Hulbert, *A time integration algorithm for structural dynamics with improved numerical dissipation: The generalized-α method*, J. Appl. Mech., 60 (1993), pp. 371–375.
[11] A. Czekanski, N. El-Abbasi, and S. A. Meguid, *Optimal time integration parameters for elastodynamic contact problems*, Commun. Numer. Math. Engrg., 17 (2001), pp. 379–384.
[12] A. Czekanski and S. A. Meguid, *Analysis of dynamic frictional contact problems using variational inequalities*, Finite Elements in Analysis and Design, 37 (2001), pp. 6861–879.
[13] P. Deuflhard, R. Krause, and S. Ertel, *A contact-stabilized newmark method for dynamical contact problems*, Internat. J. Numer. Methods Engrg., 73 (2008), pp. 1274–1290.
[14] L. C. Evans, *Partial Differential Equations*, American Mathematical Society, 1998.
[15] C. Hager, S. Hüeber, and B. Wohlmuth, *A stable energy conserving approach for frictional contact problems based on quadrature formulas*, Int. J. Numer. Methods Eng., 73 (2008), pp. 20–225.
[16] T. J. R. Hughes, *The Finite Element Method*, Dover Publications, Inc., 2000.
[17] C. Kane, J. E. Marsden, M. Ortiz, and E. A. Repetto, *Finite element analysis of nonsmooth contact*, Comput. Methods Appl. Mech. Engrg., 180 (1999), pp. 1–26.
[18] J. E. Kane, C amd Marsden, M. Ortiz, and A. Pandolfi, *Time-discretized variational formulation of non-smooth frictional contact*, Int. J. Numer. Meth. Engng., 53 (2002), pp. 1801–1829.
[19] T. A. Laursen, *Computational Contact and Impact Mechanics*, Springer, Berlin Heidelberg New York, 2002.
[20] T. A. Laursen and V. Chawla, *Design of energy conserving algorithms for frictionless dynamic contact problems*, Internat. J. Numer. Methods Engrg., 40 (1997), pp. 863–886.
[21] T. W. McDevitt and T. A. Laursen, *A mortar-finite element formulation for frictional contact problems*, Internat. J. Numer. Methods Engrg., 48 (2000), pp. 1525–1547.
[22] U. Nackenhorst, *The ale-formulation of bodies in rolling contact. theoretical foundations and finite element approach*, Computer methods in applied mechanics and engineering, 193 (2004), pp. 4299–4322.
[23] N. M. Newmark, *A method of computation for structural dynamics*, Journal of the Engineering Mechanics Division ASCE, 85 (1959), pp. 67–94.
[24] P. D. Panagiotopoulos, *Inequality Problems in Mechanics and Applications, Convex and Nonconvex Energy Functions*, Birkhäuser, Basel, 1985.
[25] M. Puso and T. A. Laursen, *A 3d contact smoothing method using gregory patches*, Internat. J. Numer. Methods Engrg., 54 (2002), pp. 1161–1194.
[26] A. Rademacher, *Finite-Elemente-Diskretisierungen für dynamische Probleme mit Kontakt*. Diploma thesis, University of Dortmund, Available via http://hdl.handle.net/2003/22996, 2005.
[27] D. Talaslidis and P. D. Panagiotopoulos, *A linear finite element approach to the solution of the variational inequalities arising in contact problems of structural dynamics*, Internat. J. Numer. Methods Engrg., 18 (1982), pp. 1505–1520.
[28] K. Weinert, H. Blum, T. Jansen, and A. Rademacher, *Simulation based optimization of the nc-shape grinding process with toroid grinding wheels*, Prod. Eng., 1 (2007), pp. 245–252.
[29] P. Wriggers, *Computational Contact Mechanics*, John Wiley & Sons Ltd, Chichester, 2002.
[30] P. Wriggers, T. Vu Van, and E. Stein, *Finite element formulation of large deformation impact-contact problems with friction*, Comput. & Structures, 37 (1990), pp. 319–331.